СООБЩЕНИЯ
ОБЪЕДИНЕННОГО
ИНСТИТУТА
ЯДЕРНЫХ
ИССЛЕДОВАНИЙ

Дубна

E13 - 6749

G.T.Adylov, F.K.Aliev, P.I.Filippov, W.Gajewski,
L.B.Golovanov, Z.Guzik, I.Ioan, I.F.Kolpakov,
B.A.Kulakov, T.S.Nigmanov, B.Niczyporuk,
V.D.Peshekhonov, E.Popielska, W.Popielski,
M.Turala, E.N.Tsyganov, D.V.Uralsky, K.Wala,
A.S.Vodopianov, Yu.V.Zanevsky
N.I.Golovnya, V.I.Kotov, Yu.S.Khodyrev,
C.Buchanan, E.Dally, D.Drickey, A.Liberman,
P.Shepard, J.Tompkins , J.Poirier

EXPERIMENTAL SETUP IN A π-e SCATTERING EXPERIMENT AT 50 GEV/C

1972

E13 - 6749

G.T.Adylov, F.K.Aliev, P.I.Filippov, W.Gajewski, L.B.Golovanov, Z.Guzik, I.Ioan, I.F.Kolpakov, B.A.Kulakov, T.S.Nigmanov, B.Niczyporuk, V.D.Peshekhonov, E.Popielska, W.Popielski, M.Turala, E.N.Tsyganov, D.V.Uralsky, K.Wala, A.S.Vodopianov, Yu.V.Zanevsky
N.I.Golovnya,[1] V.I.Kotov,[1] Yu.S.Khodyrev,[1]
C.Buchanan,[2] E.Dally,[2] D.Drickey,[2] A.Liberman,[2]
P.Shepard,[2] J.Tompkins [2], J.Poirier [3]

EXPERIMENTAL SETUP IN A π-e SCATTERING EXPERIMENT AT 50 GEV/C

[1] Institute of High Energy Physics, Serpukhov
[2] University of California, Los Angeles
[3] Notre Dame University, Notre Dame

Introduction

Elastic pion-electron scattering has been studied at the 76 GeV Serpukhov accelerator in an experiment designed to measure the electromagnetic radius of π^- -mesons. The high energy 50 GeV pion beam available at Serpukhov made such a direct measurement practical because, contrary to the situation at lower energies, the four-momentum transfer is sufficiently high so that the electron field probes dimensions comparable to the pion Compton wavelength. The aim of the experiment was to measure the pion radius with an accuracy of 5-10% [1-3]. The experimental setup was designed to record $\pi - e$ elastic scattering with high efficiency in the recoil electron energy range from 15 GeV up to the kinematic limit of 36 GeV and to utilize the highest beam intensities available for 50 GeV pions. The maximum four momentum transfer squared was about $q^2 = 0.036$ (GeV/c)^2. (Recall that $q^2 = 2m_e(E - m_e) \approx 10^{-3} E$ where E is the electron recoil energy). Since the pion radius was expected to be of the order 0.6-0.8 x 10^{-13} cm, the maximum effect of the pion form factor was expected to be 12-18% of the Mott scattering cross section so that great care in minimizing systematic errors was required.

Experimental Layout

A beam of 50 GeV π^- -mesons was incident on electrons in a 50 cm liquid hydrogen target. The main kinematic factors in this collision, that influenced the experimental setup, are shown in fig.1 which gives scattered pion and electron angles as well as the pair opening angle *vs* recoil electron energy (or q^2).

The experiment was installed in channel I2 of the Serpukhov accelerator; the setup is shown in fig. 2. It consisted of the hydrogen target, three blocks of magnetostrictive spark chambers, triggering by appropriate scintillation counters, two proportional chambers, the magnet, and two shower Čerenkov counters. Beam particles were monitored by scintillation counters $S_1 S_2 S_3 S_4$ and, upon an appropriate trigger, their tracks recorded in the five magnetostrictive spark chambers and two proportional chambers of Block I. Two scintillation counters S_p and S_e situated at the rear of the experiment after the magnet recorded the passage of a secondary π meson and an electron. For elastic scattering the pion and electron momentum must sum to 50 GeV/c; thus for a point beam of zero angular divergence, location of S_p and S_e on either side of the 25 GeV line provided an efficient trigger. Pulse heights of particles in two lead glass shower Čerenkov counters were recorded providing some electron identification. Magnetostrictive chambers in Block II in front of the magnet recorded the scattered pion and electron trajectories, those in Block III recorded their trajectories after being deflected in the magnetic field. Several anticoincidence counters were used. A_H reduced unwanted beam "halo", A-5 rejected part of the inelastic events produced in the target, and finally A_B, placed so as to intercept particles of 50 GeV/c momentum, signalled that a primary beam particle had disappeared and also helped reduce unwanted triggers from primary beam interactions in material downstream from the magnet. Counters $A_1 - A_4$ surrounded the target on four sides and were used to record inelastic interactions via latches. A 3.5 m steel muon filter was located at the rear of the experiment to aid in identification of $\mu - e$ scattering events.

The experimental equipment was arranged such that all events with recoil electron energy greater than 25 GeV were recorded with near 100% geometric efficiency and those below 25 GeV to about 15 GeV with a geometric efficiency sufficiently high that it could be accurately calculated by Monte-Carlo methods. This efficiency as a function of recoiling electron is shown in fig. 3 for a particular incident beam size and angular divergence.

Figure 4 shows a block diagram of the apparatus and its control by operators through the on-line computer. Computer output via print-out or storage-scope display generated operator responses through either push-button control panels or a teletype. The data collection system could be triggered by the fast electronic logic only when both the computer and readout electronics were in a ready state. When an event satisfying the fast logic trigger criteria occured the spark chambers were fired and spark coordinates enregistered by the readout electronics. Simultaneously, data from the proportional chambers, scintillation counters and shower Čerenkov counters, as well as certain voltage measurements were encoded. These data were then transmitted to the computer appropriately manipulated and analysed by "on-line" programs and ultimately written on magnetic tape. Results from the on-line program were presented mainly in the form of about 200 histograms that could either be displayed on a storage oscilloscope or printed on a line printer and then examined by the operator which could take control action if appropriate.

Beam

The optic of the channel preparing the beam for the target of the experimental setup is shown in fig.5a. For generation of secondary particles the aluminium target 2 mm in diameter and 20 mm long placed at the 24th magnet of the accelerator, was used. The particles with the momentum of 50 GeV/c at zero degree were taken into the channel. At the input the beam was limited by horizontal C1 and vertical C2 aperture collimators. The objective of the quadrupole Q1-Q4, connected in a doublet scheme, focused the beam into the center of the momentum collimator C3 horizontally and made it little convergent vertically. The deflecting magnet M1 with an influence of the dispersed field of the accelerator produced the momentum dispersion of the beam equal 4.4 mm per $1\%\ \frac{\Delta p}{p}$ (where Δp is the particle momentum divergence), and because the image of the target in that place was 2 mm, gave a good possibility to select the momentum range $\frac{\Delta p}{p} \geq 1\%$.

The deflecting magnet M2 compensated partially the influence of dispersion on the beam characteristics and defined the channel direction. The duplicate of the quadrupoles Q5, Q6 formed the beam of needed sizes for experimental apparatus. Its position and regime were selected to have minimum possible multiplicator coefficients of the target at the experimental setup and a small dispersion at that point. The sizes of the beam at the target at $\frac{\Delta p}{p} = \pm 1\%$ were 5.5 cm in horizontal and 4 cm in vertical (fig.6). The capture solid angle of the particles was 30 ster, and the intensity was 4×10^5 per spill at $\frac{\Delta p}{p} = \pm 1\%$ and 10^{12} of 70 GeV primary protons. The presence of the spark and proportional chambers at the experimental setup made it possible to check the momentum of the beam and its momentum divergence (fig.7). In particular, the position of the vertical image of the target at the center of the momentum collimator C3 was chosen by changing the current of the quadrupoles Q1-Q4 and measurements of the momentum divergence of particles (fig.5b).

Hydrogen Target

A 50 cm hydrogen target made by the cryogenic division of LHE in Dubna was used in the experiment /4/. The target was pressure stabilized, had special flat and windows and contained a copper foil shield which conducted bubbles around the central cylindrical region where interactions took place. This construction allows a knowledge of the amount of hydrogen path length to a precision of 0.05%.

Magnet

Momenta of secondary particles were analysed in a standard H type magnet SP-12 with a useful volume 50 cm (horizontal) x 20 cm (vertical) x 300 cm (long). Three components B_x, B_y, B_z were mapped at 70 000 points with a systematic error of order 0.1%[5]. Calibration of the Hall probe was made using NMR. These measurements were used to construct a Fourier series representation of the field, events generated by a Monte-Carlo program were integrated through the magnetic field, and the resultant momenta were fitted to obtain an expression for momentum as a function of the input and output positions and angles of particles using Tchebycheff polinomials. For the trajectories kinematically available in this experiment, the direct field integral was shown to be valid to 0.2%.

Triggering System

The experiment was triggered by a system of scintillation counters and two shower Čerenkov counters using a fast (100 MHz) electronic logic system. Information from other scintillation counters was strobed by the trigger, latched and read into the computer for further use in the analysis.

The dimensions and positions of all scintillation counters were chosen on the basis of kinematical considerations and using the known beam characteristics. All dimensions are listed below.

Counter	*Size in mm*	*Thickness in mm*
S_1 and S_2	150 x 150	5
S_3 and S_4	60 mm dia circle	5
S_e	200 x 180	10
S_p	200 x 420	10
A_H	400 x 400 with an 80 mm dia hole	10
A_5	400 x 400 with a 100 mm dia hole	10
A_B	150 x 150	10
$A_1 - A_4$	400 x 600	10
$A_1 - A_2$	500 x 250	5

The efficiency of only two of these counters, S_p and S_e, enters directly into the cross section. These two counters were each viewed by two photomultipliers, one on either side: a pulse from either phototube being considered valid by the fast electronic logic. Since both phototubes were "latched" into the computer on each event, the resultant data could be used to evaluate the counters efficiency. Voltage characteristics of these

two counters are shown in fig.8; the two phototubes are denoted by S_p, $S_{p\bullet}$ and S_e, $S_{e\bullet}$, respectively. All counters used FEU-30 photomultipliers with a resistor chain divider. The last three dynodes on all tubes were also connected to high current power supplies to prevent voltage sag during the beam spill. Voltages on each photomultiplier were sequentially measured and read into the computer.

Čerenkov Shower Counters

Two Čerenkov shower counters denoted by ACC1 and ACC2 were used in the experiment to aid in electron identification. Each was made from a block of PEMG-2 lead glass, 200 mm x 240 mm x 400 mm, the latter dimension corresponding to a thickness of approximately 12 radiation lengths. Pulse heights from the FEU-49 photomultipliers were converted by an analog-to-digital converter (ADC) and read into the computer on each event. During most of the experiment, they were also used in the trigger logic, a pulse height threshold corresponding to an electron energy of about 1/3 the minimum allowed electron energy being set for each counter. Both counters were calibrated using a 32 GeV electron beam, minimum ionizing energy muons, and ultimately electrons from observed pion-electron scattering events. The resolution of the counters is shown in fig.9 as obtained from $\pi - e$ events. During calibration the resolution was shown to be $\pm 4.5\%$ and $\pm 5.0\%$, respectively.

Fast Electronic Logic

Two parallel sets of electronic logic were used in the experiment, their agreement at the 0.5% level providing a powerful check that no mistakes were being made. One set was made from commercially available EGG, LRS and Chronetics modules; the other from modules produced in LHE at Dubna. Since high beam intensities were used, it was important to have a short spark chamber memory time. Therefore the electronics was located near the beam line at the point which minimized the time between passage of a particle through the apparatus, and development of the trigger and subsequent high voltage pulse. A delay of about 300-400 nsec was achieved.

Figure 10 shows a block diagram of the fast electronic logic. A trigger was defined by the condition

$$S_1 \cdot S_2 \cdot S_3 \cdot S_4 \cdot (S_p + S_{p\bullet}) \cdot (S_e + S_{e\bullet}) \cdot \bar{A}_H \cdot (\overline{A_5 + A_{5\bullet}}) \cdot \bar{A}_B \cdot (ACC1 + ACC2).$$

About one trigger per 10^4 mesons in the beam was produced corresponding to about 20 times the expected number of $\pi - e$ elastic interactions. The main source of backgrounds came from interactions of the beam particles in the region behind the magnet.

Spark Chambers

Two sizes of spark chambers were used in the experiment, 12 chambers 250 mm x x 250 mm and 6 chambers 420 mm x 600 mm; both with 1 mm wire spacing and both using magnetostrictive readout [6]. Chambers were arranged in three blocks. Block I, situated in front of the target, had 5 small chambers spread on a 6 m base and was used to measure the incoming pion position and angle. Block II, situated between the target and magnet, had 7 small chambers on a 5 m base and measured the scattered electron and pion positions and angles. Comparison with the first block provided a measurement of the scattering angles. Bock III, situated after the magnet, had 6 large chambers on a 4 m base and served to a measure the angles and positions of particles exciting from the magnet. A comparison with Block II gave particle momenta. One chamber in Block I, two chambers in Block II and two chambers in Block III were rotated 45° to remove ambiguities. Chamber sizes were chosen to ensure an aperture large enough to record all $\pi - e$ events with electron energy greater than 25 GeV.

Spark coordinates were readout with a conventional clock-scaler system constructed at LHE in Dubna [7]. The total number of scalers was reduced by storing pulses on an intermediate delay line; up to six sparks per plane were recorded. Chambers in Block II were read from both sides of the magnetostrictive wand to insure efficient detection of sparks separated by a distance as small as 1 mm in projection. Block I and Block III sparks could be recorded if separated by 5 mm in projection. Leading edge discrimination was used on the double wand readout in Block II; zero-crossing was used on all other chambers. Block II chambers show an additional, non-electronic, double spark inefficiency below 5 mm presumably caused by local reduction of the high voltage ("robbing"). Spark chamber efficiencies are shown in fig. 11 even for heavy loading (2-3 sparks in addition to the two $\pi - e$ sparks) efficiencies were greater than 90%. Note that the low efficiency for the last chamber (75%) is an aperture effect; many particle trajectories do not pass through this chamber.

All chamber coordinates were determined by precision surveying measurements. Positions transverse to the beam were also accurately determined by particle trajectories during periodic runs with zero magnetic field. Typical coordinate accuracies are shown in fig. 12 calculated by taking the position difference between sparks and fitted lines. Accuracy was of the order of $\pm$ 0.4 mm and $\pm$ 0.3 mm for X (high voltage) and Y (ground) planes, respectively.

Proportional Chambers

Two proportional chambers, one X and one Y, each with 40 wires and 3 mm wire spacing were used in the experiment [8]. These chambers were situated in front of the target in Block I and were used as an efficient track-finding aid since their 100 nsec memory time

is approximately ten times smaller than that of the magnetostrictive chambers. At each valid trigger from the fast electronic logic the proportional chambers were interrogated and their state sent to the on-line computer. Chamber efficiencies of 99% and resolutions of $\pm$ 1.2 mm were observed although the effective efficiency for $\pi - e$ events was reduced to 94% by dead time effects.

Readout Electronics

The readout electronics[7] was composed of control circuitry, circuitry for recording data and circuitry for transmitting the data to the computer. Fig. 13 shows the relevant block diagram. The system recorded up to 300 spark coordinates from magnetostrictive chambers, data from 80 wires of the proportional chambers, 40 latches of fast memory, the counts in 16 scalers, fixed data from input switches, and a voltage from 32 sequential points of the experimental layout. All of this information, 336 sixteen-bit words for each event, was transmitted to the HP 2116 B computer in about 2.4 msec.

Computer

All data from the experiment were collected, formatted, written onto magnetic tape, and a portion, analysed by an HP2116B on-line computer (16 bit word-length, 1.6 μsec cycle time, 32K memory, 184K eighteen msec access-time disc)[9] The computer was equipped with a teletype, fast tape reader and punch, line printer, storage oscilloscope display, disc, and two magnetic tape units. 48 input-output channels were available, not all were used. In addition to those used for conventional peripheral devices, two channels were used, one for a remote control panel used by operators for control of the experiment, the other for data transfer from the readout electronics. The computer software utilized a real-time system and could take up to 120 events per 1.8 second accelerator spill. The data were collected in a five event buffer, then written onto disc. During the 4-6 sec period between spills the data was taken from the disc, written onto magnetic tape, manipulated by analysis and histogramming programs.

On-Line Programs

All on-line programs were designed to process and provide "feed-back" for control of the experiment. Some programs also were used to give a preliminary estimation of the experimental results. Appropriate raw data from all events were presented in appropriate histograms; in addition about 30% of the events passed through a complete track-finding and analysis program. Some of the more useful histograms of raw data were

1. distribution of monitor counts for each trigger;
2. time overlap distribution of the master coincidence;
3. latches for all scintillation counters;
4. shower Cerenkov counter pulse heights;
5. spark position distributions in X and Y planes for all chambers;
6. distribution of the number of sparks in each plane.

The track-finding program reconstructed the tracks of particles in each of the three blocks independently and included a complete least-square fit to the line. Thus spark chamber accuracies, efficiencies, etc. could be observed. The most important uses of this part of the program were

1. beam characteristics (shape and momentum distribution);
2. reconstruction of $\pi - e$ events;
3. control of chamber efficiencies and accuracies.

Perhaps the most useful program of all was that which reconstructed the topology of an event enabling the operator to view events in X and Y projection on the storage oscilloscope. Figure 14 shows these views for a probable $\pi - e$ event as photographed from the display during the course of the experiment. Event number and Run number are also shown. The X view is distorted in Block III from the characteristic "V" topology by chamber shifts and the bend in the magnetic field.

Summary

Using this equipment about 3×10^6 events were recorded on magnetic tape, about 4-5% of these being identifiable as elastic $\pi - e$ scattering events. Additional information about the performance of the equipment has been obtained from the off-line analysis. Figures 15 and 16 show the accuracy of track matching in the target and the center of the magnet, respectively. These accuracies agree with that estimated on the basis of the accuracies of individual chambers. Figure 17 shows the angular match in Y (Y slope match) between Block II and Block III.

In summary the magnetic spectrometer measured angles to about $\pm$ 0.15 mrad and momenta to about $\pm$ 0.4% permitting accurate application of kinematic constraints to pion-electron scattering events. The system collected data rapidly, efficiently and precisely and permitted an accurate determination of the pion radius.

Acknowledgements

The experimental setup for the $\pi - e$ experiment has been made and put into operation by a large number of people, with the help of many divisions of the Joint Institute for Nuclear Research at Dubna, Institute of High Energy Physics at Serpukhov, University of California at Los Angeles, Institute of Nuclear Physics at Krakow.

We express our deep gratitude to the Directorate of the JINR and to A.M.Baldin, A.A.Kuznetsov, V.A.Sviridov, I.A.Savin, L.G.Makarov for their constant attention to our experiment.

We wish to thank many people from different divisions of the Laboratory of High Energies (cryogenics and energetics divisions, division of exploitation of physical apparatus, scientific electronic-experimental division, division of new scientific developments, design office, shops) and from the transport division of the JINR for their help which made this experiment possible.

We are thankful to M.I.Soloviev, Yu.G.Basha, V.N.Vinogradov and many others from the scientific-experimental division at the IHEP for their constant help in our work.

We would like to express our appreciation to the Directorate and to a lot of people from the IHEP: A.A.Logunov, R.M.Sulyaev, Yu.D.Prokoshkin, A.A.Naumov, K.Z.Tushabramishvili, E.A.Sidorov, I.A.Gusev, E.V.Eryomenko, K.P.Myznikov, A.A.Zhuravlev, V.L.Brook, A.G.Khanameryan, O.N.Radin, V.I.Bodrov and some others for creating good conditions for this joint experiment.

We are grateful to physicists M.Danysz, M.Mięsowicz, O.Czyżewski, P.Zielinski from Poland and to Professor Panofsky from the USA for supporting and encouraging this experiment.

We would like to emphasize a great contribution to this experiment of the following technicians: A.F.Elishev, B.M.Starchenko, V.A.Sutulin, A.P.Shirokov.

We would like to thank Mrs. L.N.Barabash, E.Kepa, N.Niczyporuk, J.Turala for their help in preparing our reports.

References

1. *D.Yu.Bardin et al. Investigation of the electromagnetic structure of π -meson using the IHEP accelerator. JINR report E1-4786 (1969).*
2. *A measurement of the pion charge radius by high energy pion-electron scattering. Preliminary proposal presented at IHEP-Serpukhov by Panofsky in 1969.*
3. *C.Buchanan et al. Proposal for a collaborative pion-electron scattering experiment at the 76 GeV Serpukhov accelerator. April 1970.*
4. *Yu.T.Borzunov et al. JINR report 8-5418 (1970).*

5. W.Gajewski. et al. Magnetic measurements for $\pi^- e$ experiment at 50 GeV. JINR report E13-6659 (1972).
6. G.T.Adylov et al. Magnetostrictive spark chamber system on-line with a computer in a $\pi - e$ experiment at 50 GeV/c. JINR report E13-6658 (1972).
7. Z.Guzik et al. Readout electronics for the $\pi - e$ experiment at 50 GeV/c. JINR report E1-5818 (1971).
8. Yu.V.Zanevsky et al. Multiwire proportional chambers in a $\pi - e$ experiment at 50 GeV. Nucl.Instr. & Meth., 100, 481 (1972).
9. Hewlett Pachard Computer HP 2116B, Pocket Guide.

Received by Publishing Department
on October 2, 1972

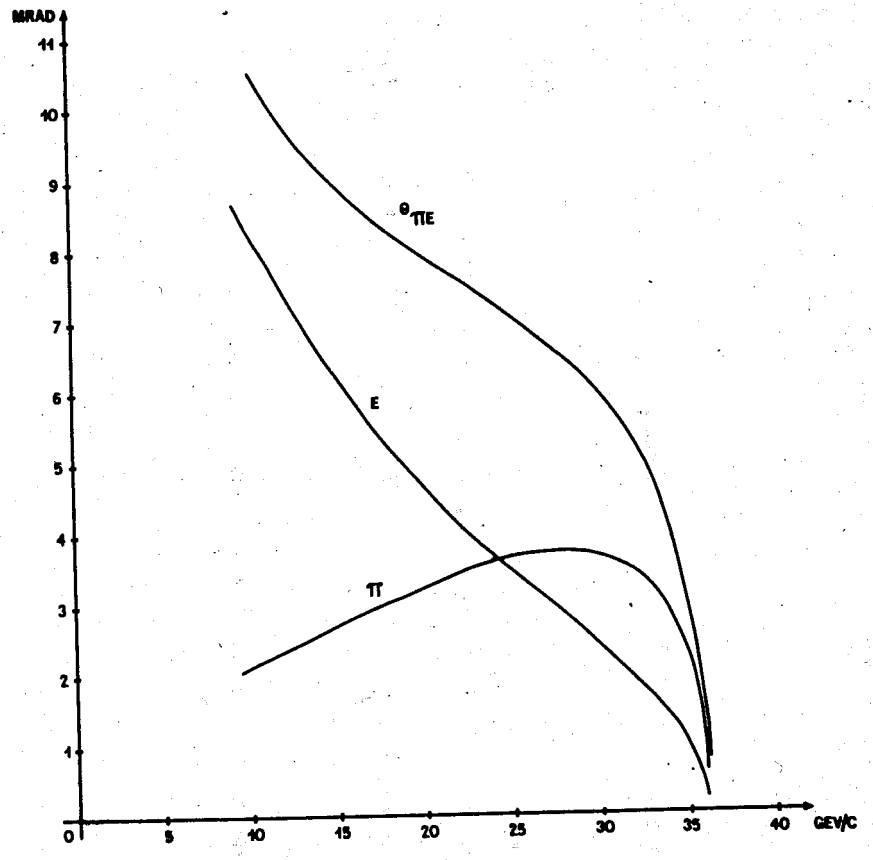

Fig.I. Scattered pion and electron angles and the opening angle of pion-electron pairs as a function of recoil electron energy for $\pi - e$ elastic scattering at 50 GeV.

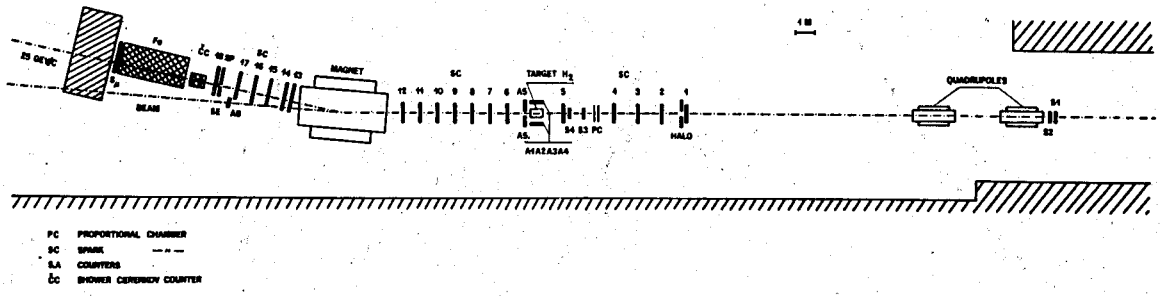

Fig.2. Experimental setup in channel 12 of the Serpukhov accelerator.

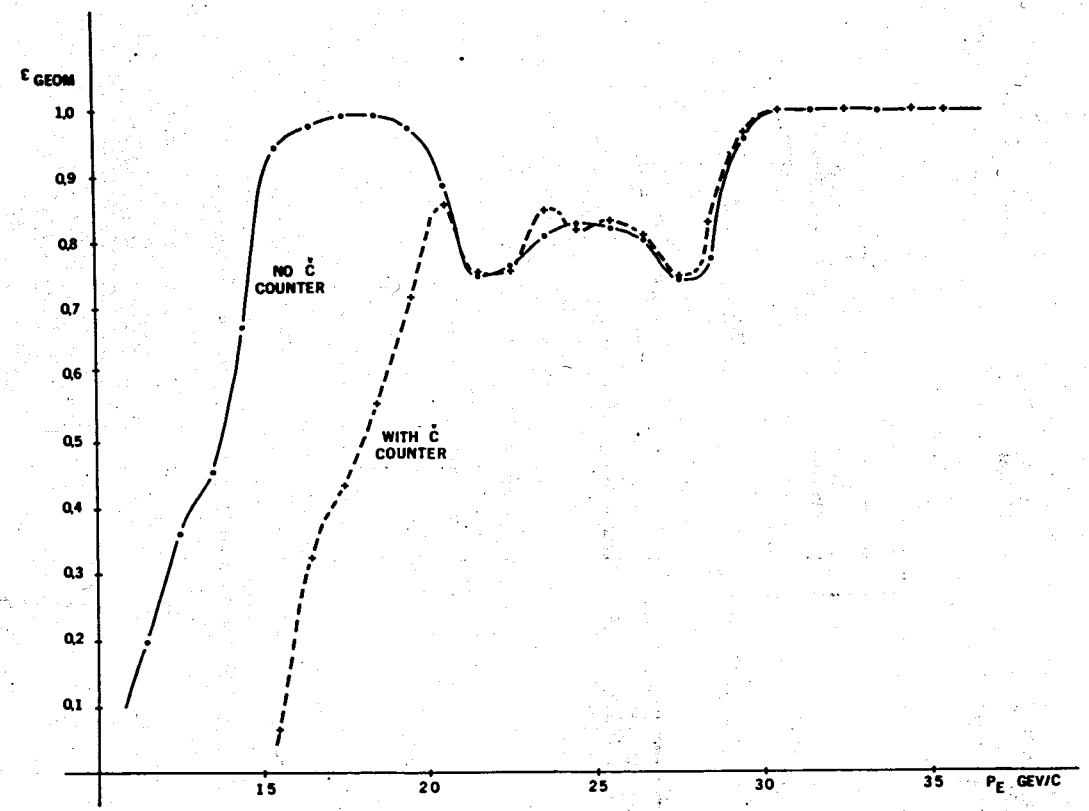

Fig.3. Geometrical efficiency for the experimental setup as a function of recoiling electron energy. Curve 1 corresponds to the trigger logic in which only S_e and S_p counters are used in coincidence with the monitor telescope.
Curve 2 corresponds to the trigger when the electron identifying shower Cerenkov counters are also used in the master coincidence.

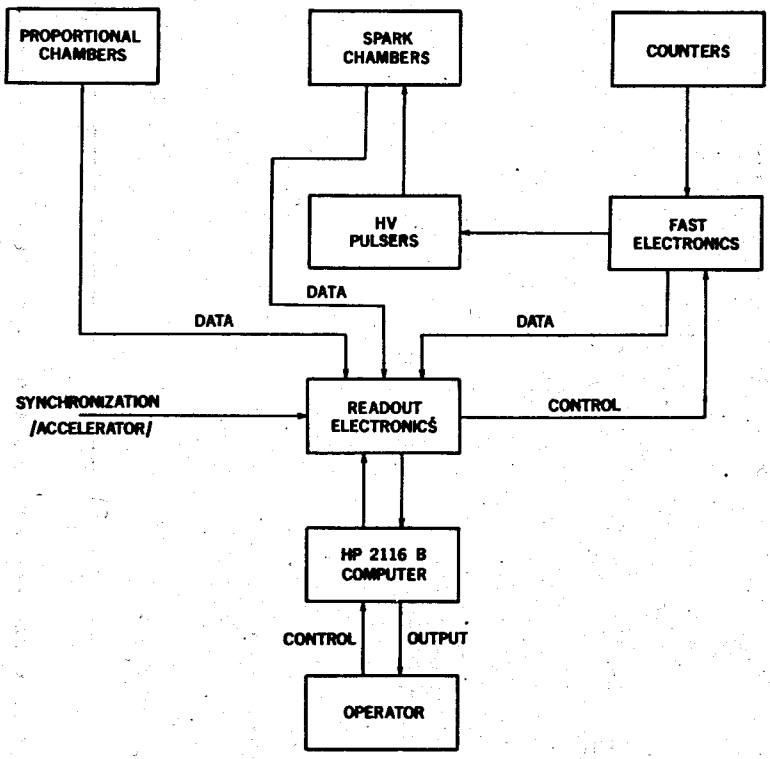

Fig.4. Block diagram of the experimental layout.

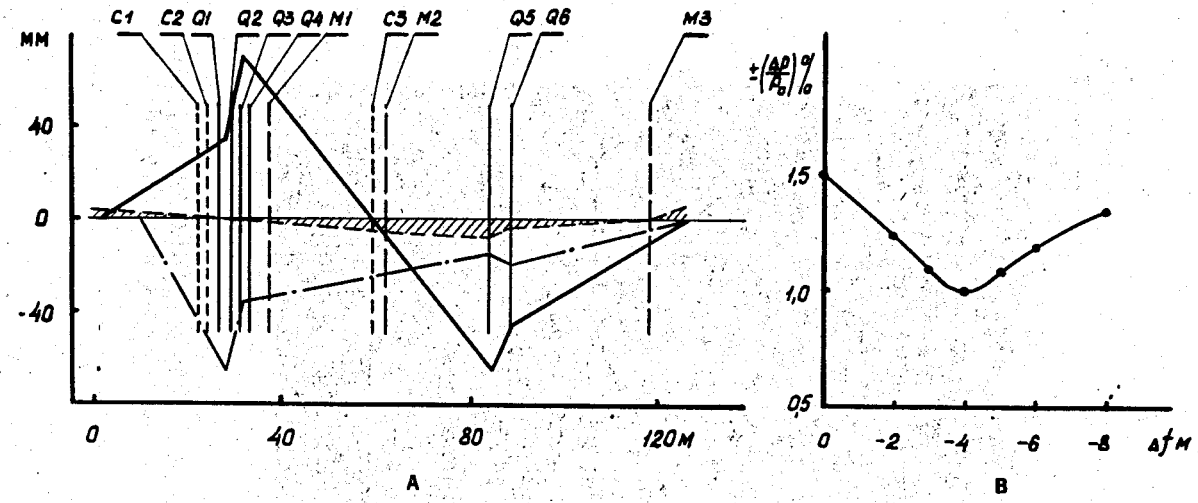

Fig.5. a)Optics of the channel and the beam in horizontal (solid line) and vertical (dash-dotted line) plane. The dispersion for $\frac{\Delta p}{p}$ = 1% is shown by the dotted line. b)The dependence of the momentum range value $\frac{\Delta p}{p}$ on the regime of the objective of the quadrupoles Q1-Q4. Along the axis the difference of the focal line from the value calculated in the horizontal plane, is set.

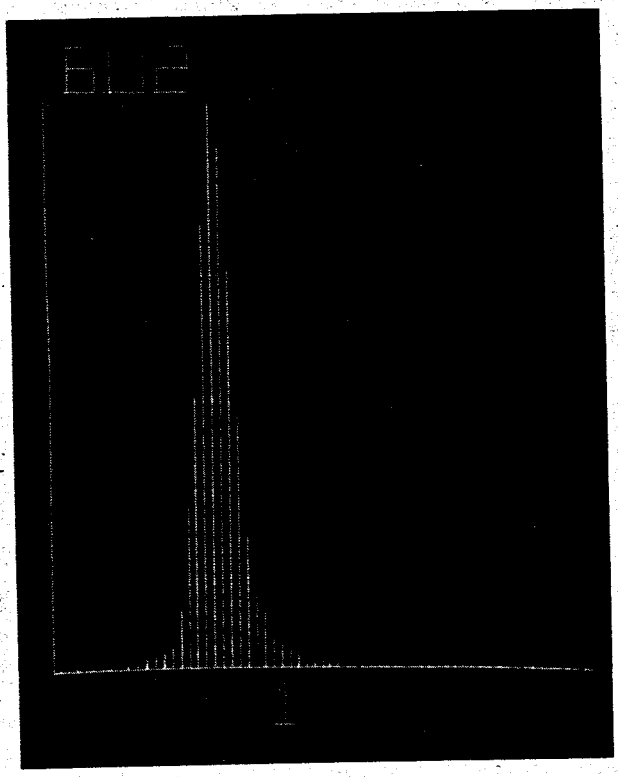

Fig. 6a. Beam profile in X view from the proportional chambers (in front of the target). Bin size corresponds to 3 mm wire spacing in the proportional chambers.

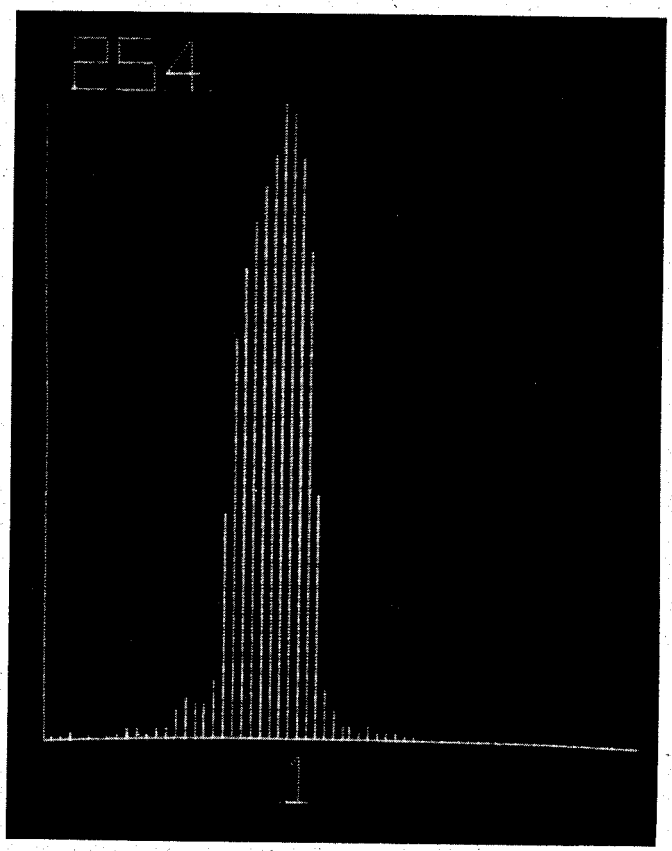

Fig. 6b. Beam profile in Y view from the proportional cgambers (in front of the target). Bin size corresponds to 3 mm wire spacing in the proportional chambers.

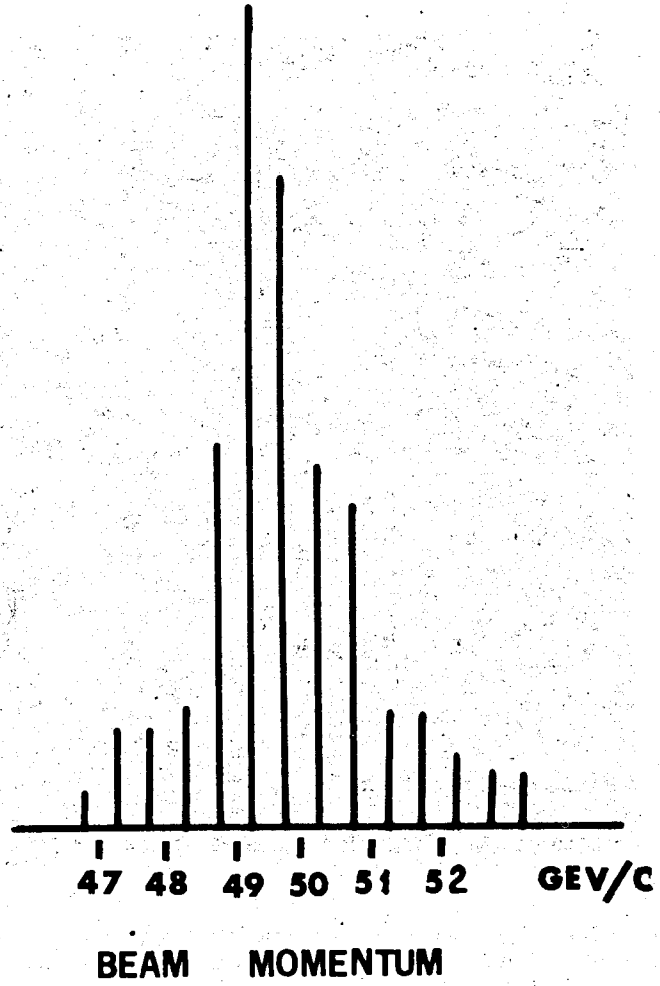

Fig.7. Beam momentum distribution measured using the spectrometer.

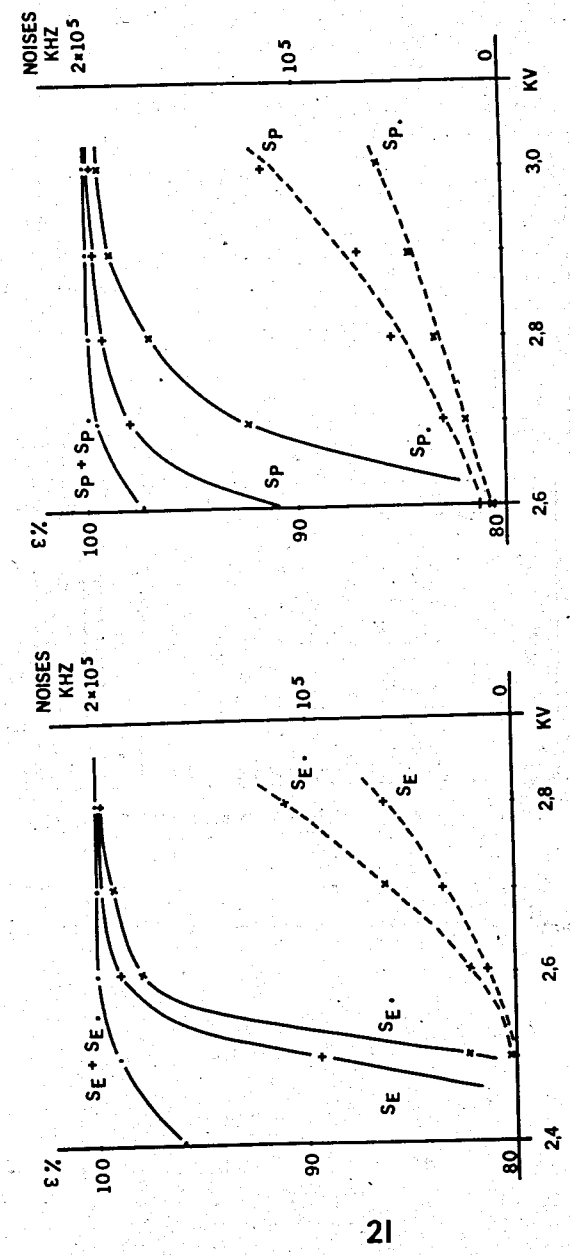

Fig.8. Voltage characteristics of S_e and S_p counters. Letters with and without dots denote phototubes located on either side of the scintillator. Solid curves show the counter efficiencies; the broken curves show the noise level.

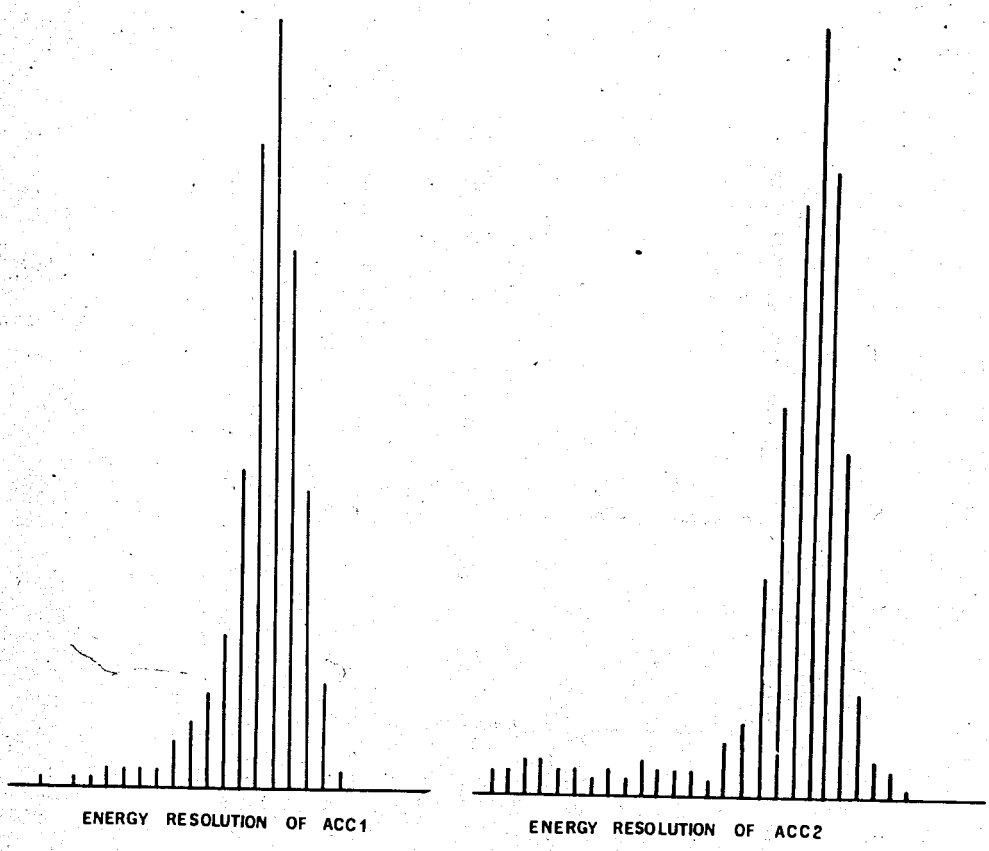

Fig.9. Shower Čerenkov counters resolution obtained from the analysis of $\pi = e$ events.

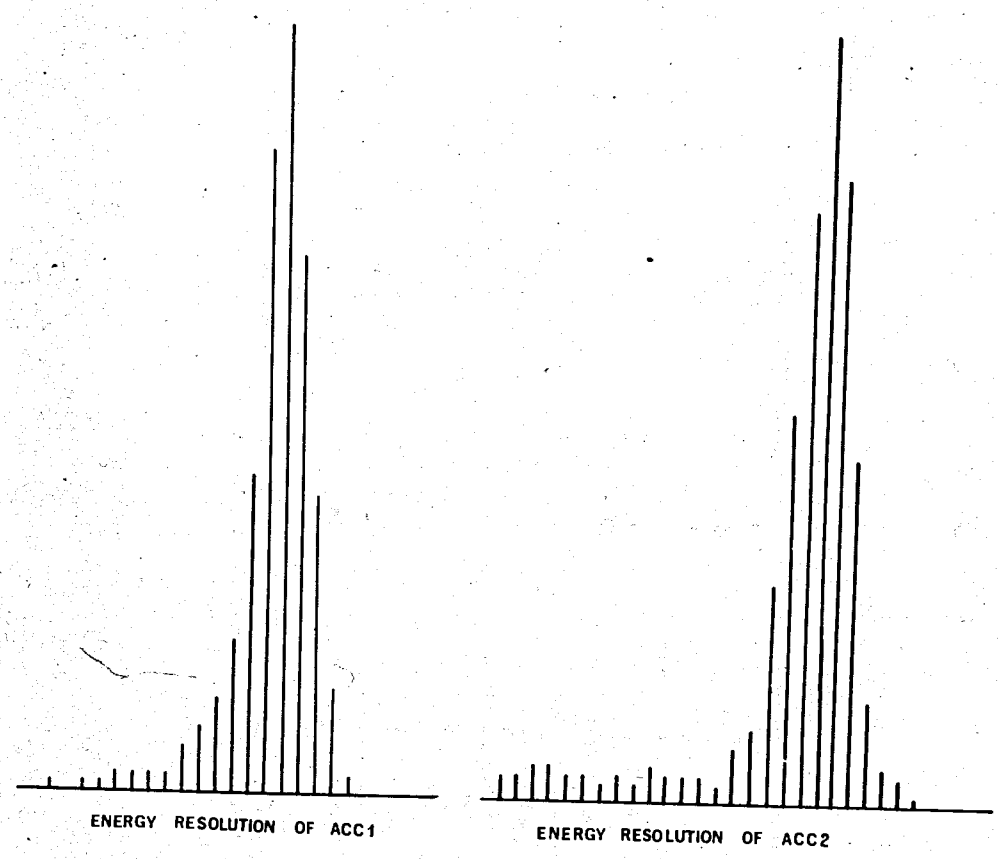

Fig.9. Shower $\overset{(-)}{\nu}$ Cerenkov counters resolution obtained from the analysis of π^{-} e events.

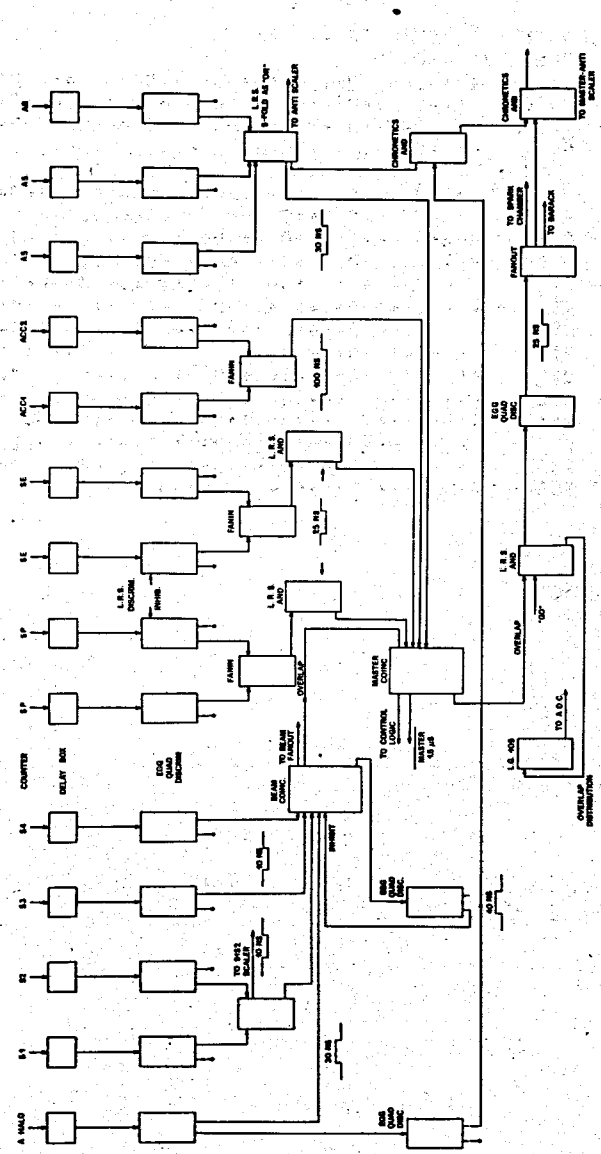

Fig.10. Electronic block diagram.

```
        TOTAL NUMBER OF ENTRIES =16427
NUMBER BELOW LOWER LIMIT10000
    1.5000     9617   ++++0++++0++++0++++0++++0++++0++++0++++0++++
    2.5000     9586   ++++0++++0++++0++++0++++0++++0++++0++++0++++
    3.5000     9780   ++++0++++0++++0++++0++++0++++0++++0++++0++++
    4.5000     9545   ++++0++++0++++0++++0++++0++++0++++0++++0+++
    5.5000        0
    6.5000     9368   ++++0++++0++++0++++0++++0++++0++++0++++0+++
    7.5000     9128   ++++0++++0++++0++++0++++0++++0++++0++++0++
    8.5000     9338   ++++0++++0++++0++++0++++0++++0++++0++++0+++
    9.5000     9774   ++++0++++0++++0++++0++++0++++0++++0++++0++++
   10.5000     9757   ++++0++++0++++0++++0++++0++++0++++0++++0++++
   11.5000     9539   ++++0++++0++++0++++0++++0++++0++++0++++0+++
   12.5000     9549   ++++0++++0++++0++++0++++0++++0++++0++++0+++
   13.5000     9160   ++++0++++0++++0++++0++++0++++0++++0++++0++
   14.5000     9629   ++++0++++0++++0++++0++++0++++0++++0++++0++++
   15.5000     9939   ++++0++++0++++0++++0++++0++++0++++0++++C++++0
   16.5000     9813   ++++0++++0++++0++++0++++0++++0++++0++++0++++
   17.5000     9752   ++++0++++0++++0++++0++++0++++0++++0++++0++++
   18.5000     9353   ++++0++++0++++0++++0++++0++++0++++0++++0+++
   19.5000     7554   ++++0++++0++++0++++0++++0++++0
   20.5000        0
   21.5000        0
   22.5000        0
   23.5000        0
   24.5000        0
   25.5000        0
   26.5000        0
   27.5000        0
   28.5000        0
   29.5000        0
   30.5000        0
NUMBER ABOVE UPPER LIMIT    0
        HISTOGRAM # 171
```

Fig.II. Spark chamber efficiencies obtained from the on-line analysis. The low efficiency of the last chamber is an aperture effect.

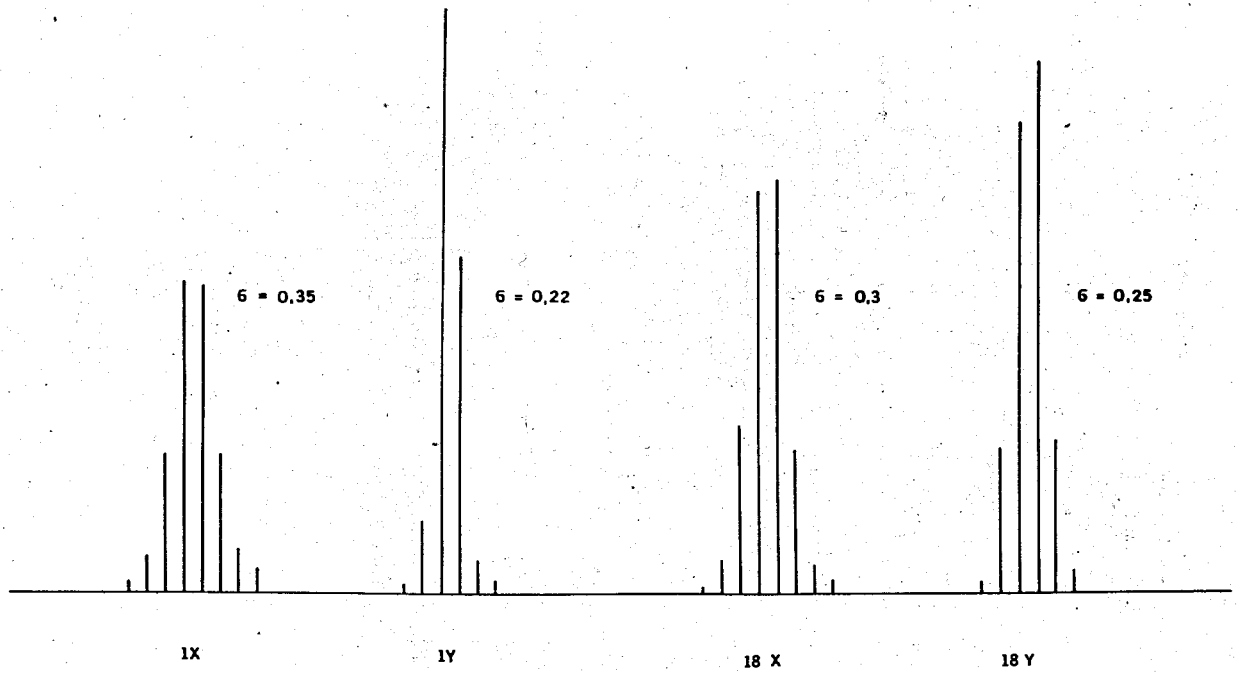

Fig.12. Coordinate accuracies for a small and large chamber calculated from position differencies between sparks and fitted tracks.

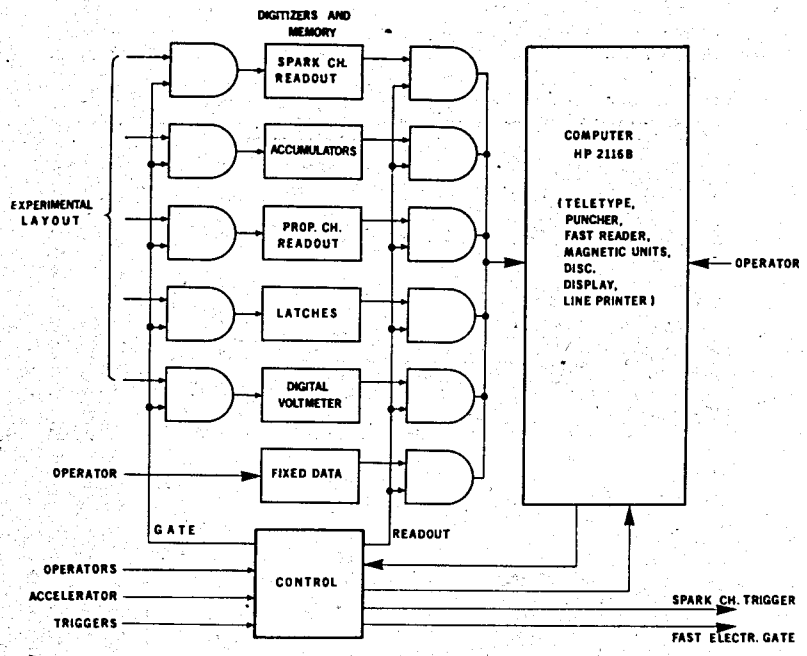

Fig.13.Readout electronics block diagram.

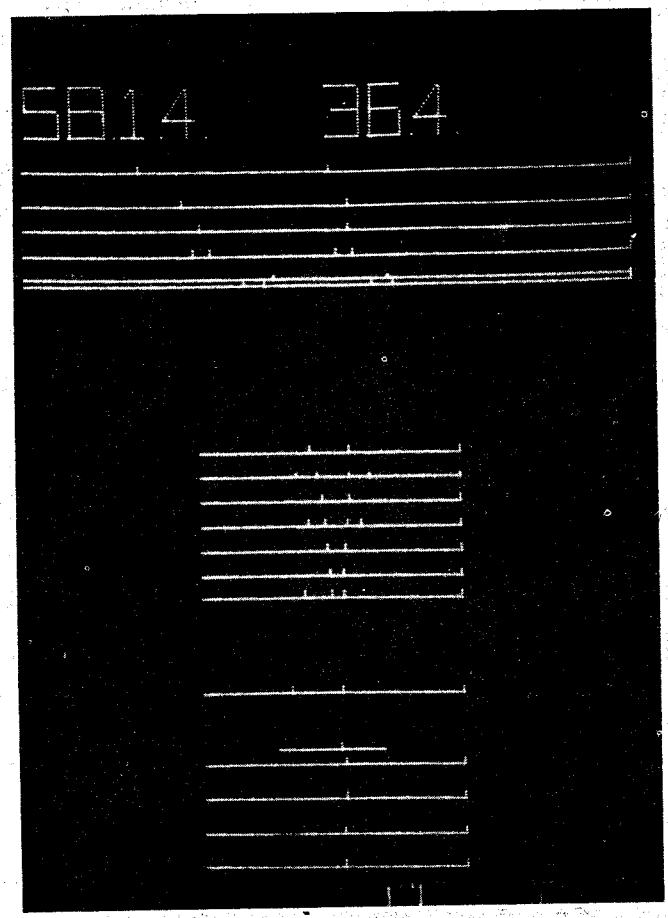

Fig. 14a. Event topology viewed on a storage oscilloscope display (*X* view).

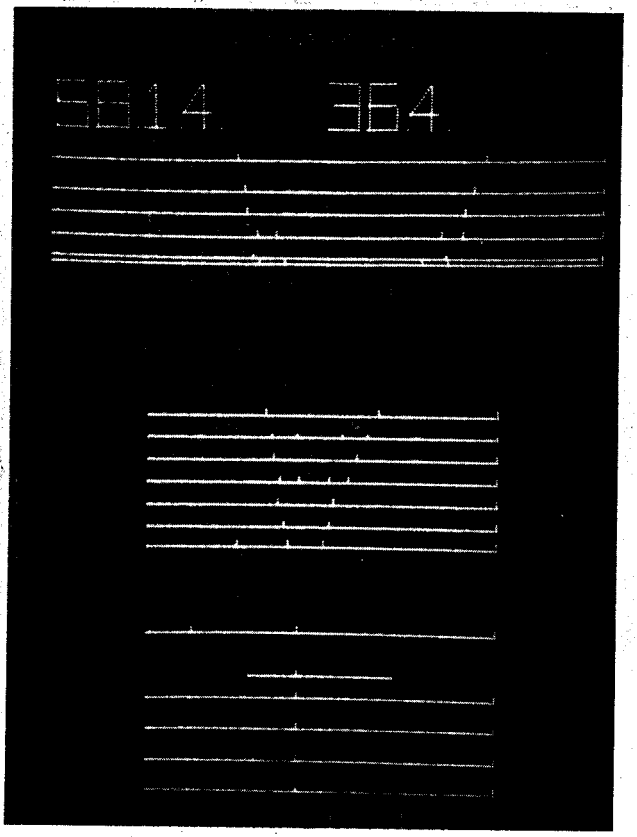

Fig. 14b. Event topology viewed on a storage oscilloscope display (Y view).

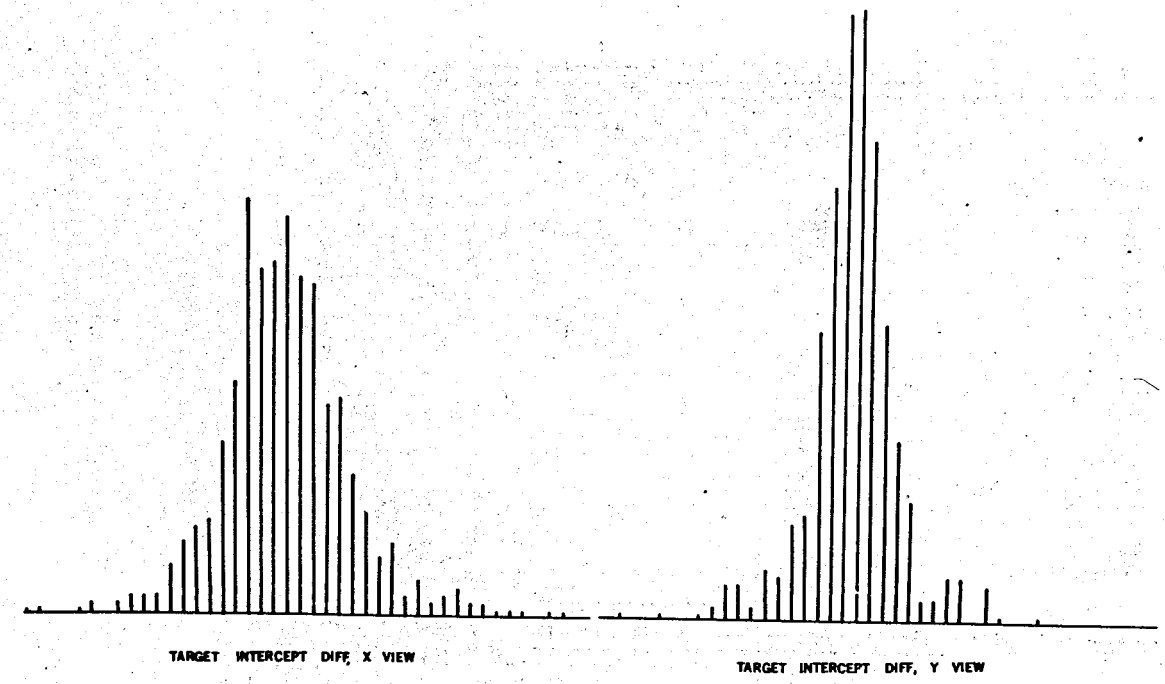

Fig.15. Spatial accuracy of track matching between the first and second blocks of spark chambers in the target. Bin size is equal to 0.2 mm.

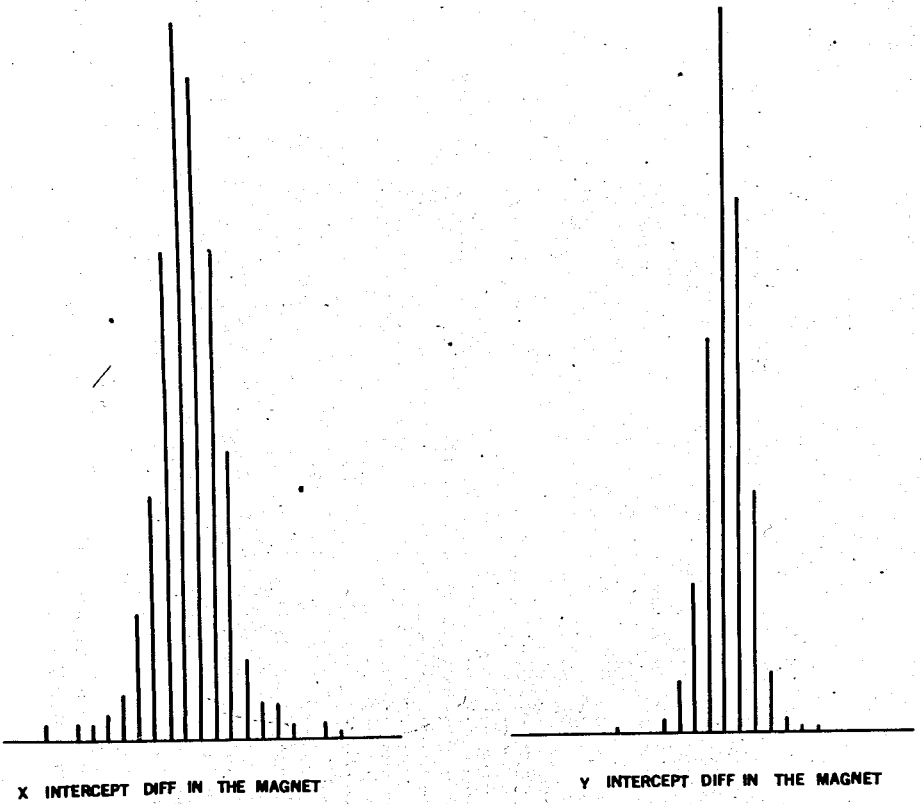

Fig.16. Spatial accuracy of track matching between the second and third blocks of spark chambers in the middle of the magnet. Bin size is equal to 0.5 mm.

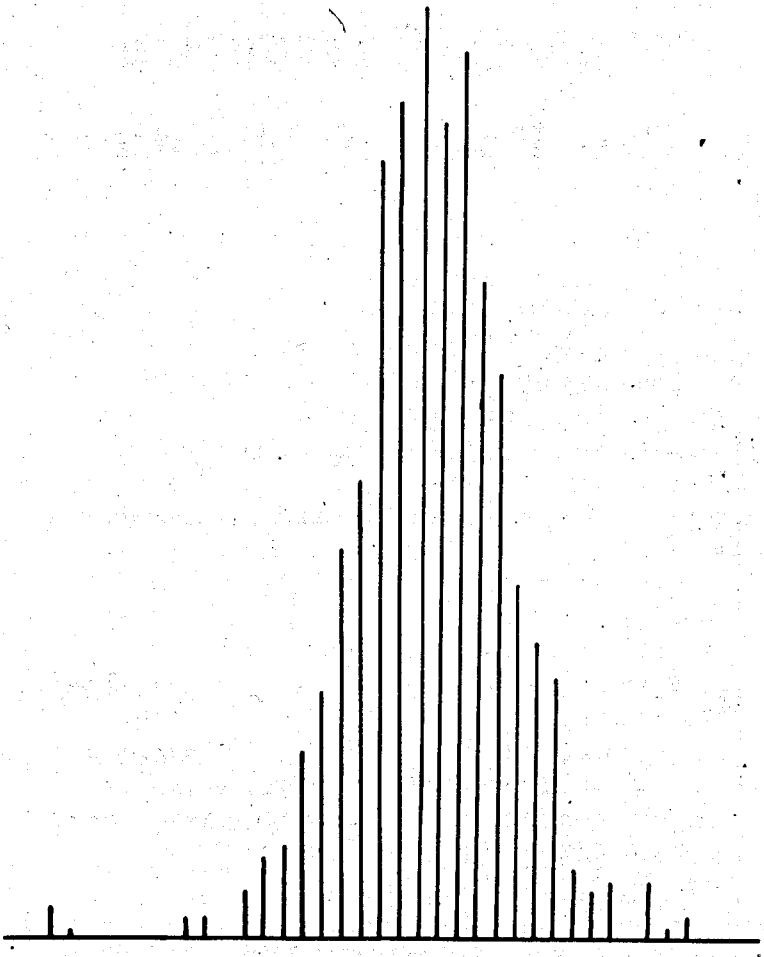

Fig.17. Angular accuracy of track matching between the second and third blocks of spark chambers in Y projection. Bin size is equal to 0.05 mrad.